Temperature measurement point optimization and experimental research for Bi-rotary Milling Head of Five-axis CNC Machine Tool

Ye Dai
Harbin University of Science and Technology
Yang Li
Harbin University of Science and Technology
Zhaolong Li (lizhaolong@hrbust.edu.cn)
Harbin University of Science and Technology
Wanjian Wen
Harbin University of Science and Technology
Shiqiang Zhan
Ningbo Tian Kong Five-Axis CNC Technology Co.

Research Article

Keywords: Bi-rotary Milling Head, Temperature-sensitive points, Neural network, Sensitivity analysis, Cooling suppression

Posted Date: April 5th, 2022

DOI: https://doi.org/10.21203/rs.3.rs-1508408/v1

Temperature measurement point optimization and experimental research for Bi-rotary Milling Head of Five-axis CNC Machine Tool

Ye Dai[1] · Yang Li[1] · Zhaolong Li[1,*] · Wanjian Wen[1] · Shiqiang Zhan[2]

[1] Key Laboratory of Advanced Manufacturing and Intelligent Technology, Ministry of Education, School of Mechanical Power Engineering, Harbin University of Science and Technology, Harbin 150000, China

[2] Ningbo Tian Kong Five-Axis CNC Technology Co., Ltd., Yuyao 315400, China

[*] Corresponding author: lizhaolong@hrbust.edu.cn

Abstract

Thermal deformation is the main factor affecting the machining accuracy of the Bi-rotary Milling Head. To accurately find out the temperature-sensitive points of the Bi-rotary Milling Head to suppress thermal deformation, this paper adopts the BP neural network sensitivity analysis method with improved connection weights to optimize the temperature measurement points, and the analysis results are subjected to randomized mean value processing to reduce the randomness of the initialization of the prediction model. The number of temperature measurement points is reduced from 15 to 4. Taking the 5AS01 Direct-drive Bi-rotary Milling Head as an example, a thermal-structural coupling model is established to analyze its thermal characteristics, and the capillary copper tube cooling suppression experiment is arranged according to the position of the temperature-sensitive points. The experimental results show that cooling the temperature-sensitive points can simultaneously reduce the thermal error in X and Z-directions by about 58%, providing a basis for the Bi-rotary Milling Head to improve machining accuracy.

keywords Bi-rotary Milling Head · Temperature-sensitive points · Neural network · Sensitivity analysis · Cooling suppression

1. Introduction

The Bi-rotary Milling Head (hereinafter referred to as milling head) is the core part of the five-axis NC machine tools. It is mostly used to process complicated surfaces such as impeller and propeller, which reflects the manufacturing level of high-end equipment. Compared with the three-axis machine tool, the five-axis machine tool has two more rotating axes, which can be more flexible for surface processing with higher precision. So it can complete multiple processing procedures in one clamping [1], reducing the positioning errors caused by multiple clamping and improving the accuracy of the workpiece. Due to the influence of multiple heat sources during the machining process, a non-uniform temperature field is formed inside the milling head, resulting in a different temperature rise of each component, which in turn generates different degrees of thermal deformation and ultimately affects the machining accuracy of the machine tool. Some experiments show that the thermal error caused by thermal deformation accounts for 40 ~ 70% of the total error [2]. To obtain higher machining accuracy, this paper investigates the temperature field and thermal errors of the milling head and performs cooling suppression for some temperature-sensitive points.

The internal structure of the milling head is compact, and a large amount of heat will accumulate to generate thermal deformation under high-speed operating conditions. At present, many domestic

and foreign scholars have conducted in-depth and extensive research on the thermal characteristics of the milling head. Since the thermal error is affected by several factors such as temperature gradient, cooling system, and ambient temperature, it presents time lag, time variation, and nonlinearity [3], it is difficult to construct an accurate mathematical model according to its mechanism, so it is usually described by finite element simulation analysis and data-driven thermal error prediction model. Sun [4] simulated the temperature field diagram of the milling head, and the high temperature is mainly concentrated in the motorized spindle. When the spindle is running, the high-speed rotation of the spindle and its transmission chain provides the main heat source for the temperature change of the milling head [5], resulting in a significant increase in the temperature of the spindle, A-axis, and C-axis. To analyze the spindle thermal error closely related to the bearing thermal characteristics, Liu et al. [6] proposed a motorized spindle unit analysis and modeling method based on thermal-fluid-structure coupled finite element simulation to predict the thermal characteristics of the motorized spindle. Lin [7] used finite elements to analyze the C-axis transmission part of the milling head and found that the torsional deformation of the spacer has a great influence on the C-axis transmission.

In addition to finite element simulation, many scholars also conduct thermal network analysis based on the mechanism or build a neural network prediction model to predict thermal error. Zhou et al. [8] combined the thermal-mechanical coupling effect to strengthen the thermal network model of the motorized spindle based on thermal resistance, and the average relative error of the prediction results was less than 8%. Ke et al. [9] combined the thermal network method for thermal transient analysis of the main shaft and considered time-varying parameters and thermal-structural coupling. To make the thermal error prediction model with high accuracy, scholars have proposed various modeling approaches, such as neural networks, support vector machines, gray system theory, optimization algorithms, etc. Guo et al. [10] proposed an artificial bee colony neural network (ABC-NN) modeling method to train the connection weights and used them for the prediction of the thermal error of the main axis. Abdulshahed et al. [11] proposed an adaptive neuro-fuzzy inference system (FCM-ANFIS) with fuzzy c-means clustering to optimize the model parameters by changing the number of inputs and the number of membership functions. Wu et al. [12] used a convolutional neural network to build a C-axis thermal error prediction model, extracted and learned the features of the C-axis thermal image, and predicted the positioning error under different temperature conditions, with an accuracy of more than 90%. Various modeling methods have shortcomings such as prematurity and a large amount of calculation. To solve this problem, Li et al. [13] proposed an algorithm that integrates artificial fish swarm algorithm, ant colony algorithm, and neural network, combined with the thermal deformation and temperature data of the five-axis machine tool spindle to build an online prediction model for the thermal deformation of the spindle. In these studies, the establishment of the model requires the acquisition of temperature data through temperature sensors. Too many sensors will lead to complex models, and too few sensors will make it difficult to ensure model accuracy.

As the world enters the era of big data, scholars pay more and more attention to data analysis. Data sensitivity analysis methods are mainly divided into two sensitivity analysis methods based on mathematical statistics and neural networks. Tunkiel et al. [14] proposed a data-driven sensitivity analysis method based on machine learning models, but over-reliance on input data. Arnst et al. [15] Used mathematical statistics to obtain probabilistic representations of elastoplastic material properties and subsequently determined which features had the greatest impact on the deformed shape based on stochastic sensitivity analysis. Guo et al. [16] combined the Morris method in mathematical statistics and the grey correlation analysis method to determine the weight coefficient of the geometric error

compensation value to correct the comprehensive model. The research methods of neural network local sensitivity analysis mainly include partial derivative-based, connection weight-based, and perturbation-based methods. Jiang et al. [17] combined the randomization test method with three neural network sensitivity analysis methods respectively, and analyzed the neural network prediction model, so as to determine the main factors affecting the output change of the prediction model. To reduce the disturbance of the initial data, Yang et al. [18] proposed a neural network thermal error prediction model that could identify the key thermal stiffness of the machine tool, construct a temperature transfer matrix per unit temperature rise, and judge the key thermal stiffness of the machine tool according to the value of thermal error variation. These studies showed that the two sensitivity analysis methods can accurately calculate the sensitive terms of the model and accurately characterize the model with fewer parameters.

Some of the above-mentioned analysis processes are mainly based on the finite element method to analyze the thermal performance of the milling head, find out the serious heating parts, and build a mathematical-statistical or neural network prediction model to predict the thermal error. But they neglect to screen out temperature-sensitive points for cooling suppression. When the neural network model has many parameters or the relationship between the parameters and the output is nonlinear, it is more difficult to get accurate results by the sensitivity analysis method based on mathematical statistics. However, due to the complex thermal deformation mechanism of the milling head and the nonlinear relationship between the parameters and the output, the sensitivity analysis method based on mathematical statistics is not suitable for analyzing the thermal error model of the milling head.

This paper is mainly aimed at the problem that the temperature rise of the milling head shell (hereinafter referred to as shell) causes the thermal error at the end of the motorized spindle, constructs a mathematical model of the neural network to describe the shell thermal deformation, uses the sensitivity analysis algorithm to calculate the sensitivity of the input data, and then combines the randomized mean value method to reduce the fluctuation of the sensitivity coefficient and optimize the selection of temperature-sensitive points. Finally, the cooling suppression experiment is arranged according to the temperature-sensitive points and the cooling effect is verified.

2. Thermal characteristics analysis of milling head

2.1 The mechanical structure of the milling head

The milling head mainly includes the A/C axis, motorized spindle, shell, and some connecting parts. This paper takes the 5AS01 direct-drive milling head as the research object, and its structure is shown in Fig. 1. The high-speed motorized spindle and rotor are connected by interference, and the torque of the built-in motor is transmitted to the spindle. The built-in motor power is large, the stator and rotor generate heat seriously. Therefore, a cooling water sleeve is installed outside the built-in motor. The shell is the mounting base for the main parts of the milling head and the motorized spindle, and the motorized spindle is fixedly connected to the A/C axis, where the C-axis can achieve ±360° rotation around the Z-axis and the A-axis drives the motorized spindle to swing around the X-axis at ±110°. By adding two degrees of freedom to the machining center, the five-axis linkage can be realized to complete the machining of complex surfaces with high precision.

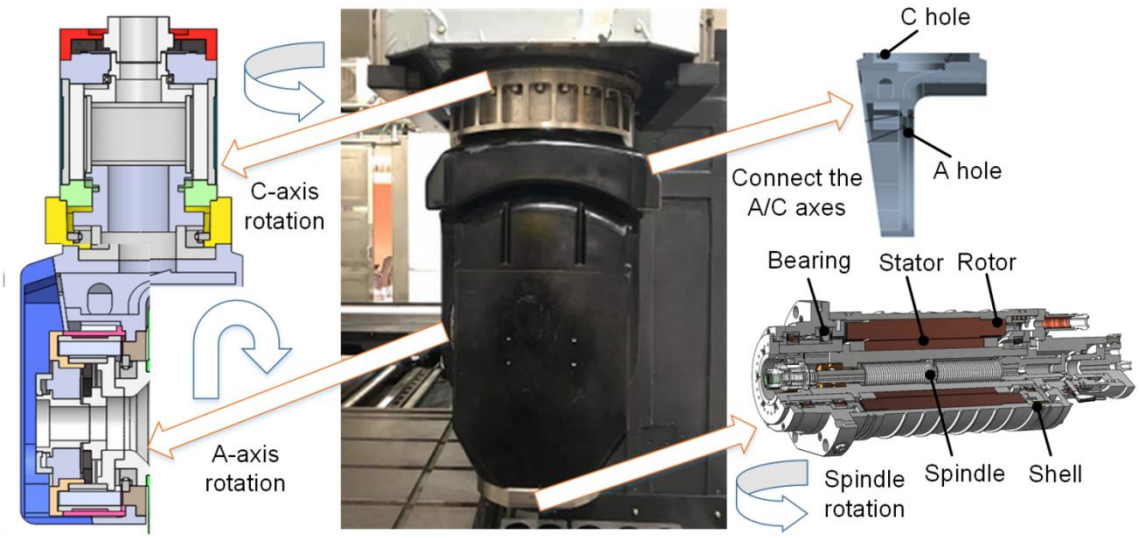

Fig. 1 Overall structure of the milling head

2.2 Calculation of thermal boundary conditions

The direct-drive milling head is directly driven by a torque motor, so the heat source mainly considers the heat generation of the motor and ignores the heat generation of the bearing and the cutting heat. The motor heat mainly includes the heat generation of the A-axis, C-axis motors, and the motorized spindle motor. The A-axis motor is directly connected to the shell, and the C-axis motor rotor is connected to the shell through the connecting piece. The heat generation can be calculated by Eq (1). Since the temperature of the external environment remains constant, the heat generated inside the milling head is mainly exchanged through heat conduction and heat convection. Heat conduction can be calculated by setting parameters in the software. Heat convection is divided into natural convection and forced convection. The convective heat transfer coefficient [19] can be calculated according to Eq (2).

$$q = \frac{Q}{V} \tag{1}$$

In the formula: q is the heat generation rate (W/m^3); Q is the thermal power (W); V is the volume of the heat source (m^3).

$$h = \lambda \cdot \frac{Nu}{L} \tag{2}$$

In the formula: λ is the thermal conductivity of the fluid(W/(m·K)), Nu is the Nusselt number, L is the characteristic size of the exothermic wall surface (m).

According to Eq (1) and (2), the thermal boundary conditions of the milling head can be obtained, as shown in Tables 1 and 2:

Table 1 Heat generation rate of each heat source of milling head

Heat source	Heat generation rate (W·m^3)
Spindle motor	2256107.7
A-axis motor	2765389.3

C-axis motor	1995180.9

Table 2 Convection heat transfer coefficient

Location	Type of convection	Convective heat transfer coefficient (W/(m^2·K))
Shell	Natural convection	5
Spindle water sleeve	Forced convection	1244
Spindle shell	Natural convection	9.7
A-axis water sleeve	Forced convection	1357.3
A-axis shell	Natural convection	5
C-axis water sleeve	Forced convection	1621.9
C-axis shell	Natural convection	6

2.3 Analysis of temperature field of milling head

The 3D model is imported into the ANSYS platform, and the finite element analysis of the milling head is performed after setting the material parameters and thermal boundary conditions. At rated speed, the steady-state temperature field results of the milling head and shell are shown in Fig. 2(a). After the temperature field of the milling head reaches a steady state, the highest temperature is located at the rotor axis of the motorized spindle, which can reach 78.054 °C, followed by the rotor of the C-axis and A-axis motors respectively. As the internal structure of the motorized spindle is more compact, the airflow heat dissipation effect is poor, and there is no cooling water for heat dissipation, so its temperature is the highest. Although the heat generated by the stator accounts for 2/3 of the heat generated by the motor, the cooling water sleeve installed outside the motor stator can effectively reduce the temperature, making it much lower than the rotor. The A/C axis motor has a larger shaft center space, the heat dissipation effect is better, and less heat generation than the motorized spindle, so the temperature rise is relatively lower.

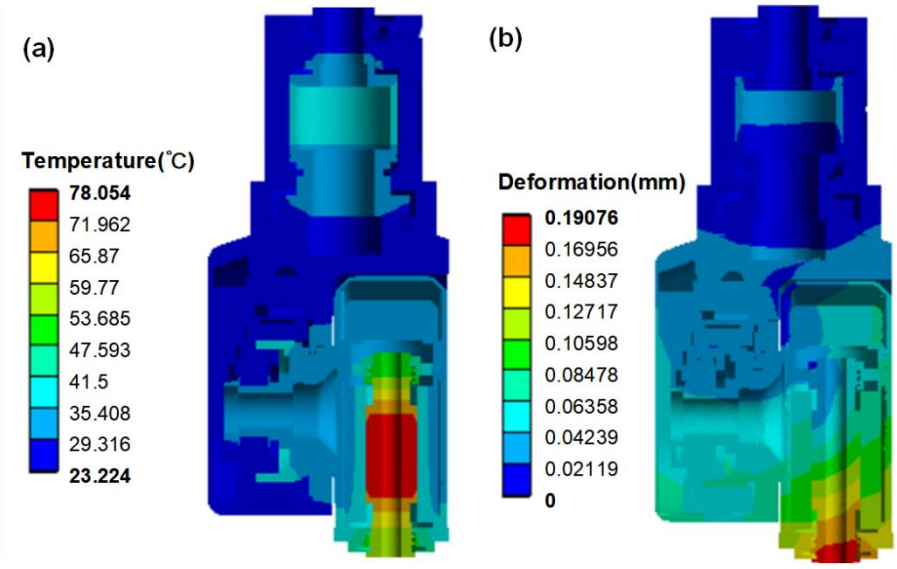

Fig. 2 Milling head finite element simulation analysis **(a)** Temperature field **(b)** Thermal deformation field

As the largest connecting piece in the milling head, the shell is connected to the main heat source and has a high temperature rise. The highest temperature is at hole A where the shell is connected to the A-axis, and the temperature of hole A is low above and high below. The variation of the maximum temperature at the milling head, shell and heat source is analyzed. As shown in Fig. 2(a), the highest temperature of the milling head tends to be stable after 1600s, but the highest temperature of the shell tends to be stable after 6400s, which is because the motorized spindle rotor with the highest temperature in the milling head is not directly connected with the shell, and the cooling water sleeve is arranged outside the stator of the motorized spindle, which further slows down the heat transfer to the milling head.

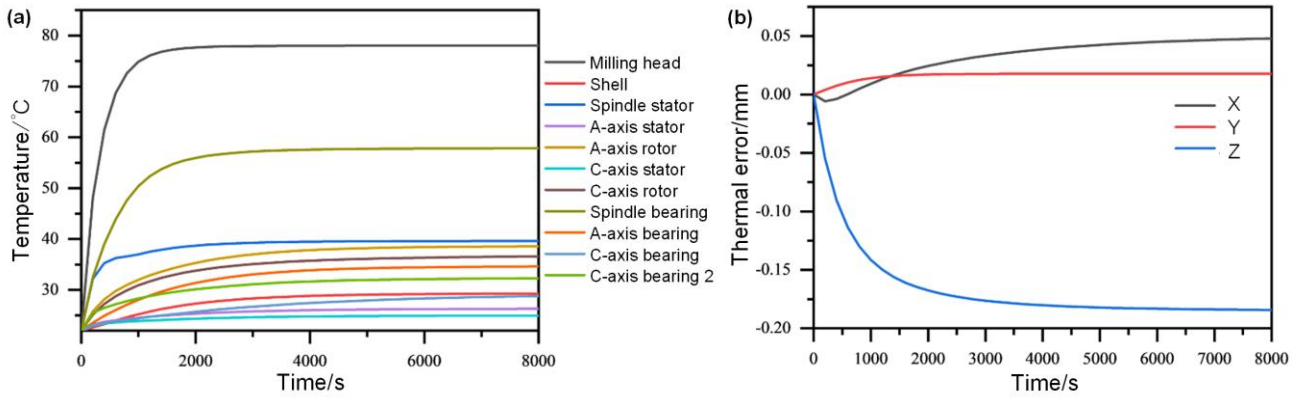

Fig. 3 **(a)** Maximum temperature variation of each part of the milling head **(b)** Transient thermal error at the end of the motorized spindle

2.4 Analysis of thermal deformation field of milling head

The maximum thermal deformation of the milling head (in Fig. 2(b)) is located at the end of the motorized spindle, which is 0.19076mm. From the temperature field of the milling head, it can be seen that the temperature of the motorized spindle core is the highest, so the transient thermal error diagram of the motorized spindle end is derived. As shown in Fig. 3(b), the thermal error in Y-direction reaches a stable and minimum value quickly, and tends to be stable after about 2500s; Z-direction thermal error is the largest, and tends to be stable after about 6400s; X-direction thermal error is stable and the slowest, and the thermal error first changes along the X-negative direction, and then change along the positive direction. From the analysis, it can be concluded that the motorized spindle Z-direction and X-direction thermal error are the main error sources of the milling head.

5AS01 model milling head is an offset direct-drive milling head with a symmetrical structure in the Y-direction. The Y-direction maximum thermal error is located at the side of the shell and is symmetrical. As can be seen from Fig. 3(a) and Fig. 3(b), the Y-direction thermal error stabilization time of the motorized spindle is much earlier than the maximum temperature smoothing time of the shell. So the Y-direction thermal deformation of the shell has a small effect on the thermal error of the milling head and can be ignored. The asymmetry between the X and Z-direction has a great influence on the thermal error of the milling head. Among them, the Z-direction thermal error is the largest, and the Z-direction thermal error stabilization time is consistent with the highest temperature stabilization time of the shell. So the Z-direction thermal deformation of the shell has a great influence on the thermal error of the milling head. The high-speed motorized spindle has high power and serious heat generation. When the heat is gradually conducted to the shell, hole A is thermally expanded, resulting

in a larger X-direction deformation, so the X-direction thermal error is large.

3. Thermal deformation experiment and sensitivity analysis algorithm

The robustness of the model is affected due to errors in temperature acquisition and linear coupling between different temperature measurement points. To ensure the accuracy of the input of the Back Propagation (BP) neural network model, temperature-sensitive points are selected from 15 temperature measurement points. First, the heating experiment is carried out to collect temperature and thermal displacement data, and the influence of thermal deformation on the thermal error of the motorized spindle is analyzed. Then, based on the sensitivity analysis method of improving connection weights, the temperature-sensitive points are optimized and selected, and the points with higher sensitivity coefficients are used as temperature-sensitive points for cooling suppression.

3.1 Heating experiment

As the largest connection of the milling head, the shell is connected to the three motors on the milling head at the same time, and the change of its temperature field and thermal deformation field will have a direct impact on the displacement of the tool tip, which results in a large machining error. Therefore, the heating experiment is performed on the shell.

3.1.1 Experimental scheme

The whole experiment uses 15 PT100 temperature sensors and two eddy current displacement sensors. Using the temperature real-time monitoring device and the position real-time monitoring device to transfer the collected data to the computer, the software accompanying the collector controls the sampling frequency and records the data, and the overall process of the heating experiment is shown in Fig. 4.

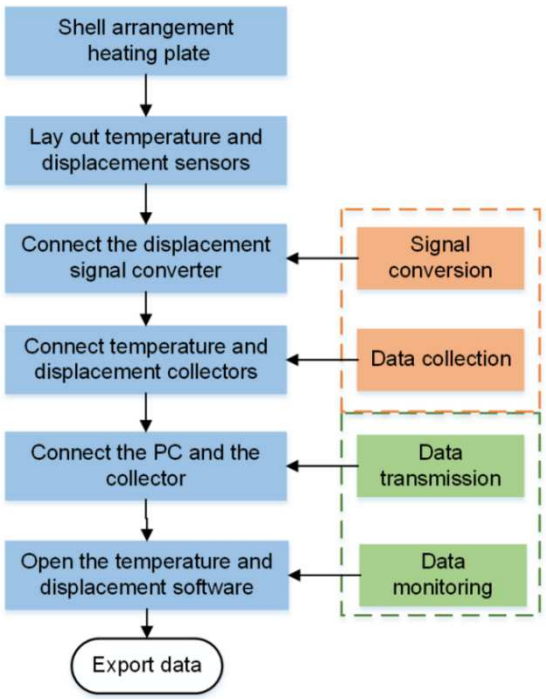

Fig. 4 Heating experiment process

Figure 5 shows the overall experimental setup and the position of the displacement sensor. Two eddy current sensors are used to measure the thermal displacement data, where X_1 measures Z-direction thermal displacement, X_2 measures X-direction thermal displacement. The temperature detection points of the shell are shown in Figure 6(a). The heat source detection points are T5, T6, T7, and T14, the air detection point is T15.

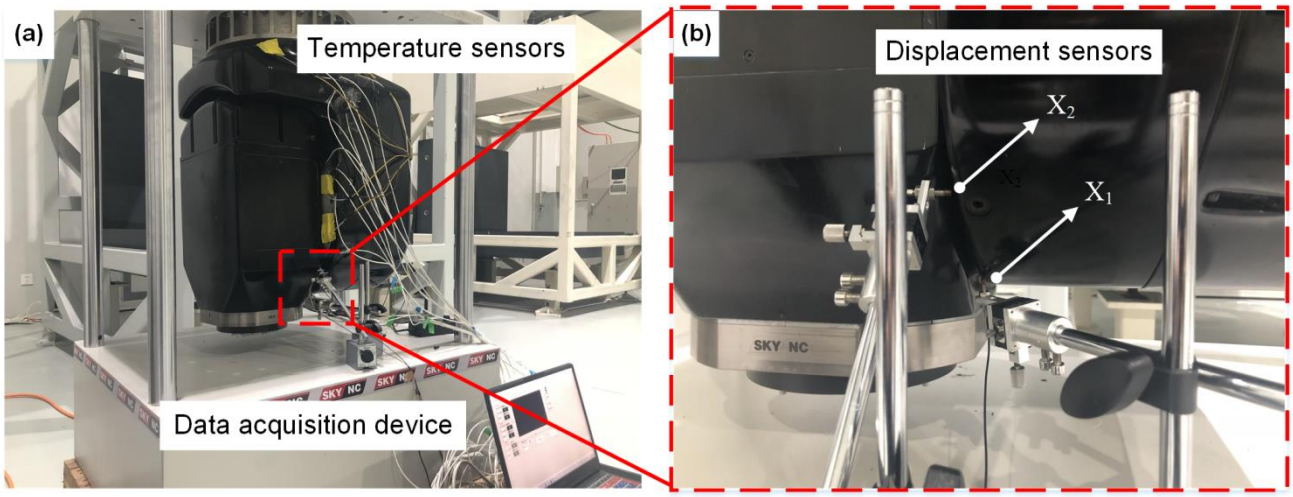

Fig. 5 **(a)** The experimental setup **(b)** Location of the two displacement sensors

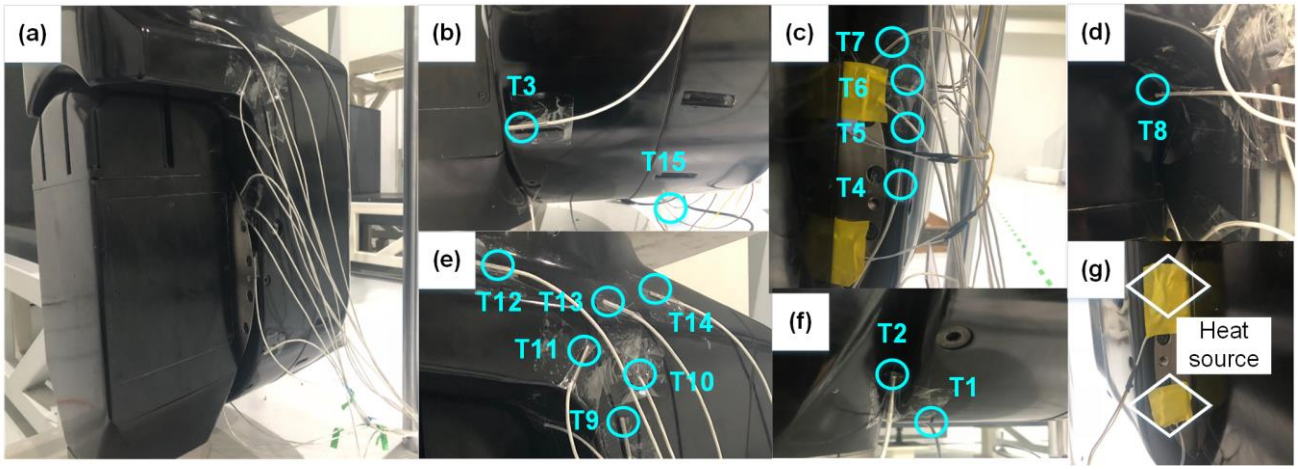

Fig. 6 **(a)** All temperature sensors on the Milling Head **(b)** Temperature sensor arranged on the side of the shell **(c)** Temperature sensors arranged near the heat source **(d)** Temperature sensor arranged outside hole A **(e)** Temperature sensors arranged near hole C **(f)** Temperature sensors arranged at the bottom of the shell **(g)** Heat source

3.1.2 Experimental results and data analysis

The experiment is set to sample the temperature and displacement data at an interval of 5s, at which time the temperature and displacement data of each detection point tend to be stable, and the temperature data are organized as shown in Fig. 7(a). The contact area between the shell and the C-axis is large, and the heat is easily transferred, while the contact area with the A-axis is relatively narrower, so the temperature of T6 is higher than the temperature of T14 under the same voltage. Among the non-heat source detection points, the temperature rise of the detection point near hole A is relatively higher than that of other points, especially at the bottom of the shell (T1), the maximum temperature rise can reach 5°C. The analysis is due to the high temperature caused by the structure of

the shell itself. The highest temperature location in the temperature field simulation is the bottom position of hole A (T2), but in the experiment is lower than T1, T3, T4, which is because the heat failed to transfer to the back cover faster in the heating experiment, so the temperature of these three points is higher.

The thermal displacement change curves at X_1 and X_2 are shown in Fig. 7(b), and the X and Z-directional displacements measured by the displacement sensor grow negatively. After the shell is heated for 5.5 hours, the maximum thermal error in the Z-direction reaches about 0.034mm, and the maximum thermal error in the X-direction reaches 0.014mm. So the Z-direction thermal error in heating experiment is much larger than the X-direction, which is consistent with the conclusion from the thermal deformation simulation analysis and verifies the accuracy of the simulation analysis.

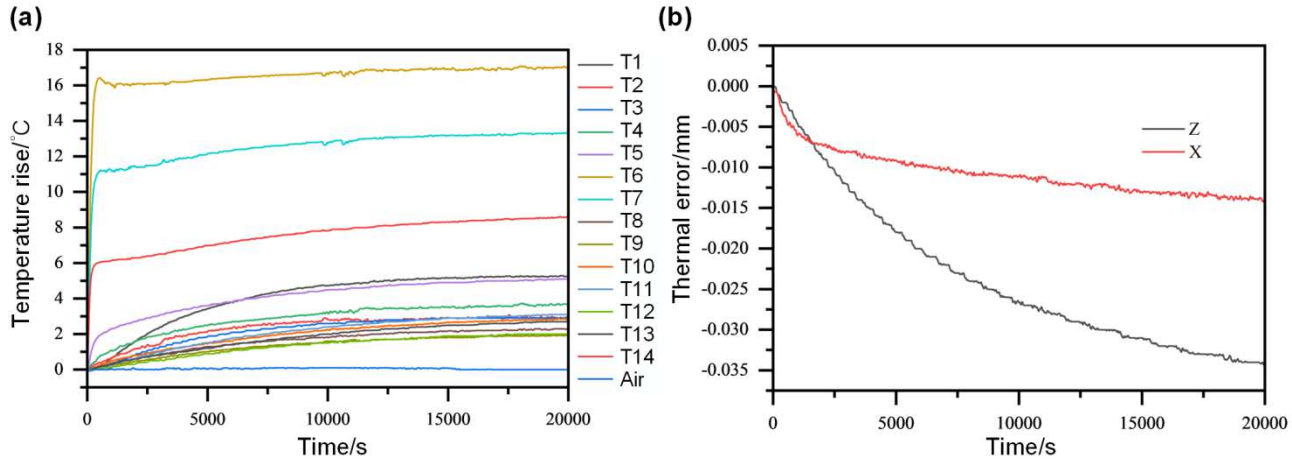

Fig. 7 **(a)** The temperature rise of each detection point in the heating experiment **(b)** The thermal displacement change of the heating experiment

3.2 Temperature measurement point optimization

3.2.1 BP neural network

The neural network is a mathematical model imitating bionic nerves, and its design parameters mainly include the number of network layers, the number of neurons in the input layer, hidden layer, and output layer. It can realize complex nonlinear mapping and is suitable for solving problems with internal mechanisms. A single hidden layer BP neural network is used to construct the thermal error prediction model of the part, which reduces the number of parameters of the neural network and the uncertainty of the model. The BP neural network has n inputs, k outputs, and j hid layer neurons. Where x^t_n is the n-th input of the t-th sample of the neural network, b_1 and b_2 are the biases, and the functions $f(\cdot)$and $g(\cdot)$ use the Sigmoid function as the activation function of the hidden layer and output layer. The w_{nj} is the weight from the input layer to the hidden layer, v_{jk} is the weight from the hidden layer to the output layer, the update formulas of w_{nj} and v_{jk} are as Eq (3).

$$\begin{cases} w_{nj} = w_{nj} + \eta\alpha_j^t(1-\alpha_j^t)x_n\sum_{k=1}^{K} v_{jk}e_k \\ v_{jk} = v_{jk}\eta\alpha_j^t e_k \end{cases} \tag{3}$$

where η is the learning rate and e_k is the output expectation.

The input q^t_j of the *j-th* neuron in the hidden layer under the *t-th* sample generates the output α^t_j under the action of the hidden layer function, that is

$$\alpha^t_j = f(q^t_j) = f(\sum_{n=1}^{N} w_{nj} x^t_n + w_{0j} b_1) \tag{4}$$

The input r^t_k of the *k-th* output neuron of the *t-th* sample generates the output result y^t_k under the action of the output layer function, that is

$$y^t_k = g(r^t_k) = g\{\sum_{j=1}^{J} v_{jk} f(\sum_{n=1}^{N} w_{nj} x^t_n + w_{0j} b_1) + v_{0k} b_2\} \tag{5}$$

3.2.2 Sensitivity analysis method based on improved connection weights

Sensitivity analysis can quantitatively evaluate the impact of changes in model input variables on the output results and is an effective way to reveal the laws embedded in the model. To accurately water-cool the parts with severe heating of the shell, so that the cooling effect can reach the best and reduce thermal deformation, this paper uses the BP neural network combined with the sensitivity analysis method to screen out the temperature-sensitive points for cooling. Firstly, the shell heat source detection points (T5, T6, T7, T14) and air detection point temperature data are excluded, and the neural network prediction model is constructed with the temperature and displacement detection point collection data. Then the BP neural network prediction model is subjected to sensitivity analysis using the sensitivity analysis method based on connection weights, and the sensitivity coefficients in the detection points are sorted.

Among the sensitivity analysis methods, the Garson algorithm [20] is relatively classic, which mainly calculates the sensitivity coefficient of the input parameters according to the weights in the BP neural network. The disadvantage is that the positive and negative effects of the weights are ignored, which leads to the deviation of the final calculation results. The improved sensitivity analysis method can reflect the positive and negative correlation between input and output, and the sensitivity coefficient [21] $S_{nk,olden}$ of this method can be obtained by Eq (6). It is assumed that the neural network has *N* input layer neurons, *J* hidden layer neurons, and *K* output layer neurons.

$$S_{nk,olden} = \frac{\sum_{j=1}^{J} w_{nj} v_{jk}}{\sum_{n=1}^{N} \sum_{j=1}^{J} w_{nj} v_{jk}} \tag{6}$$

Due to the randomness of BP neural network initialization, there will be some concatenation in the output sensitivity coefficient results, and the instability caused by random initialization needs to be weakened. To make the calculation result stable, the randomized mean value method is finally introduced, that is, the mean value of multiple sets of data is taken after randomizing the parameters. The steps are as follows:

(1) Determine the BP neural network structure. The nodes of the input layer are temperature-sensitive points, and the nodes of the output layer are their respective sensitivity coefficients.

(2) Initialize the grid and related parameters of the model, and input the data of temperature-sensitive points for training.

(3) Calculate the sensitivity of neural network input based on the sensitivity analysis method of improved connection weights.

(4) Repeat steps (2) and (3) 2000 times

(5) Calculate the overall mean of the sensitivity coefficient and the effect of each result on the mean value, evaluate whether the sensitivity coefficient is stable, output and sort.

(6) Repeat steps (1) to (5) 3 times. Output the results of the three randomized mean processing and verify the sensitivity ranking accuracy. The randomized mean processing procedure is shown in Figure 9.

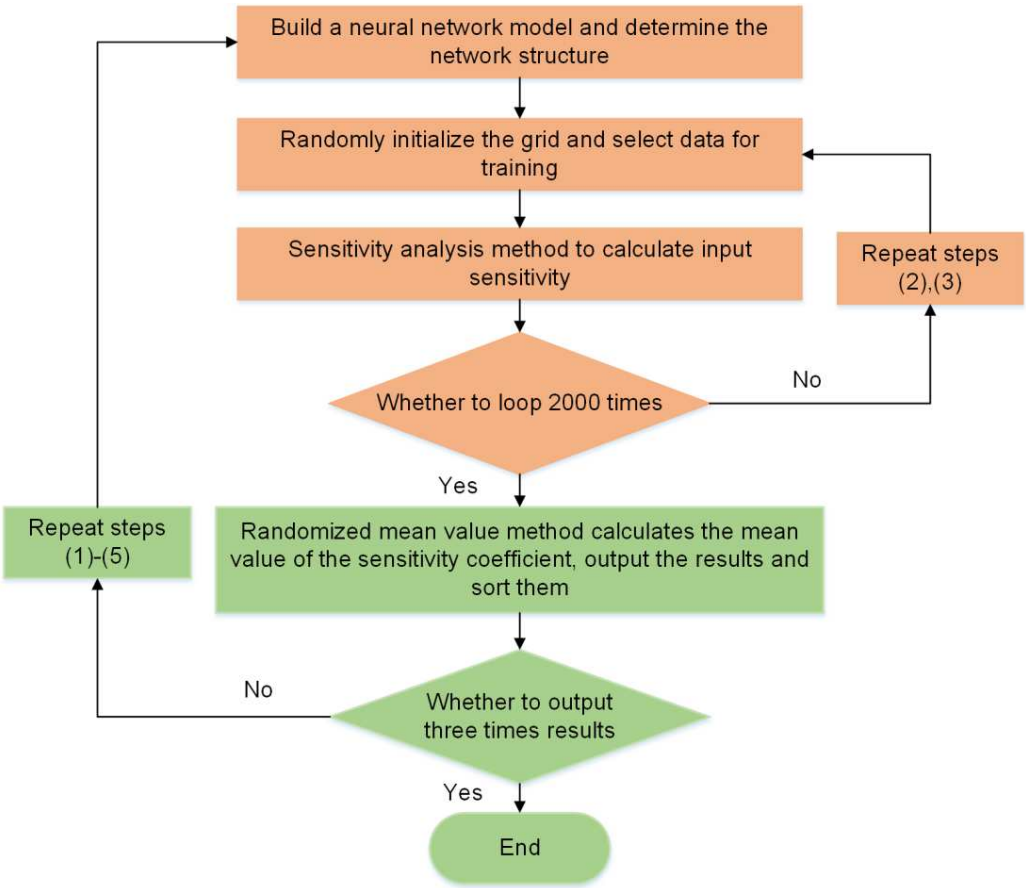

Fig. 8 Steps of randomized mean value method for sensitivity coefficients

The sensitivity coefficient of the input temperature is calculated by MATLAB combined with Eq (6), and the model is subjected to random mean value processing. After 2000 calculations and three randomization averages, the fluctuations are significantly reduced. Derive one of the Z and X-direction sensitivity coefficient calculation results, as is shown in Fig. 10, in the initial stage, the Z-direction and X-direction sensitivity coefficients fluctuated greatly. After 600 calculations, the overall fluctuation is small, and after 2000 calculations, it becomes stable. The results of the three randomized mean values are shown in Table 3. It can be seen from the table that the fluctuation of the ranking of the sensitivity coefficients also becomes smaller after adopting the randomized mean value method, and the values of the sensitivity coefficient points T1, T4, T8, and T11 are higher, while the sensitivities of T3, T2, and T12 are lower, and the results of the three calculations are basically the same.

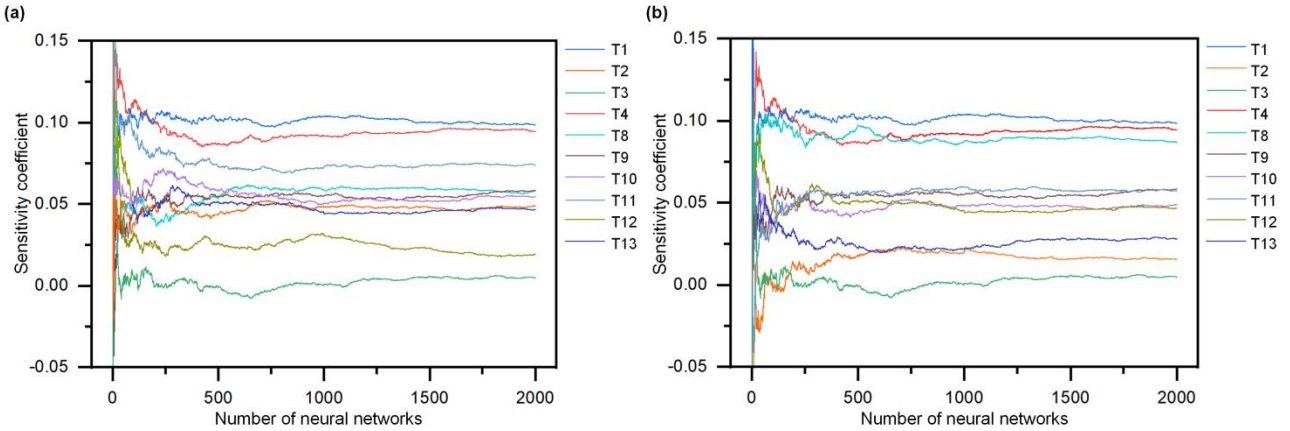

Fig. 9 Calculation of mean sensitivity coefficients based on improved connection weights **(a)** Z-direction sensitivity coefficient **(b)** X-direction sensitivity coefficient

Table 3 Z-direction and X-direction sensitivity coefficient

Sensitivity coefficient	Z			X		
High	T1	T1	T1	T1	T1	T1
	T4	T4	T4	T4	T4	T4
	T11	T11	T11	T8	T8	T8
	T8	T8	T8	T11	T11	T11
	T10	T9	T9	T9	T9	T9
	T9	T10	T10	T12	T10	T10
	T2	T2	T2	T10	T12	T12
	T13	T13	T13	T13	T13	T13
	T12	T12	T12	T2	T2	T2
Low	T3	T3	T3	T3	T3	T3

4. Cooling suppression experiment

Combined with temperature measurement point optimization results, the cooling positions of T1, T4, T8, T11 points with high sensitivity coefficients and the less sensitive T3 points are selected for cooling. Before conducting the experiment, a capillary copper tube cooling experiment is carried out to prepare the cooling suppression experiment. Capillary copper tube using W-shaped, O-shaped, and straight tube ways to cool the iron block, and eventually find that the cooling effect of the straight tube is better than the W-shaped and O-shaped capillary copper tube, so the cooling experiments of the capillary copper tube using the straight tube way to carry out.

4.1 Experimental scheme

The cooling system mainly includes a water cooler, flow meter, ball valve, capillary copper tube, and relief valve, which are connected as shown in Fig. 11. The water cooler uses air cooling to ensure the temperature of the cooling water, making the temperature of the cooling position close to room temperature and reducing the temperature gradient difference. The outlet end is connected to a flow

meter to detect the magnitude of the flow rate. The two ends of the ball valve are connected to the flow meter and the capillary copper pipe connector to control the size of the flow of coolant into the capillary copper pipe. The length of the capillary copper tube is about 80mm, and there are two snap rings inside the joint to effectively prevent coolant leakage. The pipeline is connected with a relief valve to prevent coolant leakage due to excessive pressure in the pipeline. The PC internal and external threads are used to connect the pipelines between each part.

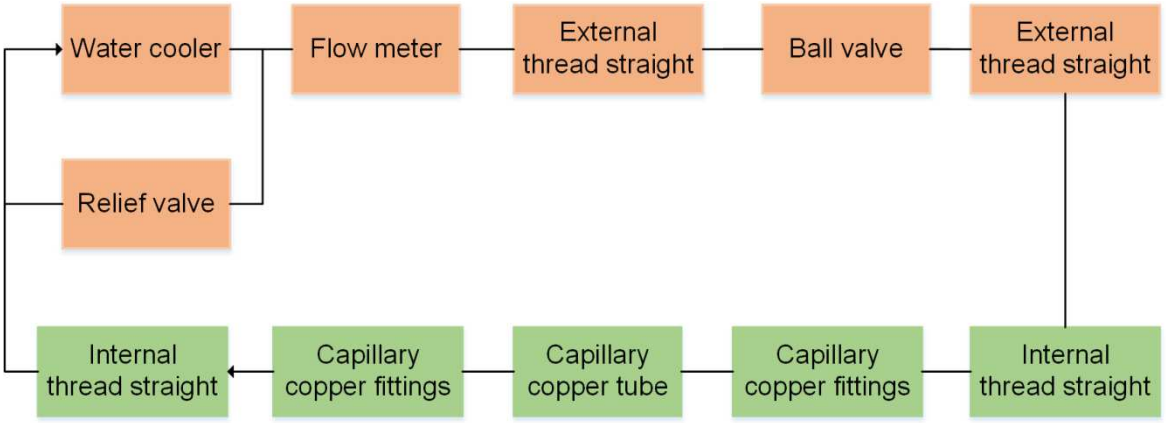

Fig. 10 Cooling experimental instrument connection

To compare the temperature changes more clearly, and consider the installation arrangement, the cooling positions are all near the temperature-sensitive points, and the locations of the five cooling points finally selected are shown in Fig. 12. The copper tube is installed with heat-conducting silica gel at contact with the shell to play the role of heat transfer uniformity and vibration damping. Before the experiment, it is detected that the vibration of the displacement detection point caused by the capillary copper tube flowing water is less than 0.7 um, which can be ignored.

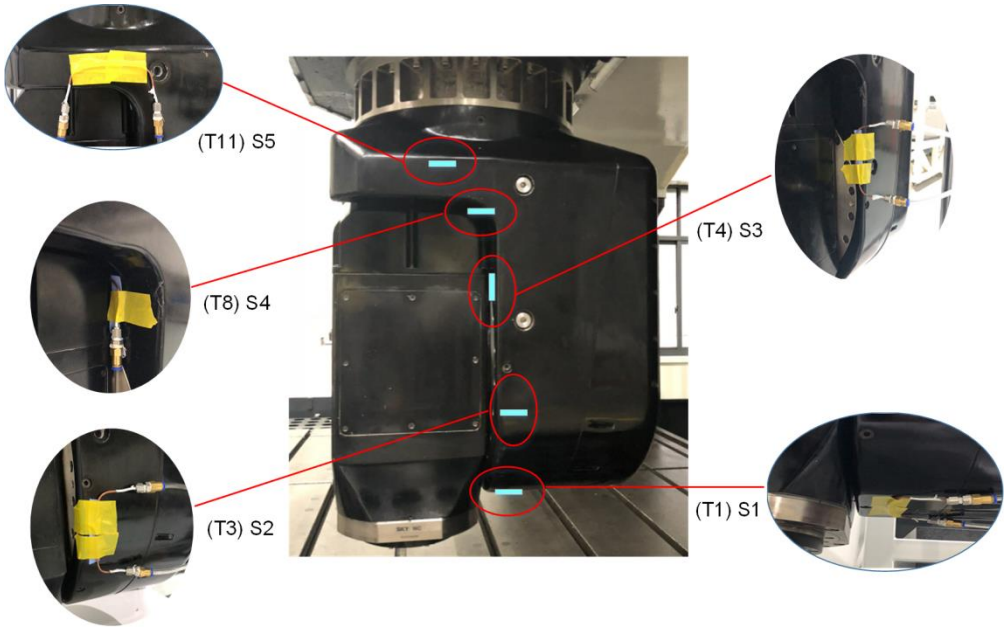

Fig. 11 Five cooling point locations in the cooling experiment

For the convenience of comparison, S0 is set as the experiment without cooling, and the thermal error data of 6 groups of experiments are compared. From Fig. 13(a) and (b), it can be seen that S1 has the best effect, which can reduce the thermal error in both X and Z-direction by about 58%. If only

X-direction is considered, the effect of S3 is better. Compared with the heat source arrival time, the S3 point has a great influence on the thermal error because it is close to the heat source and is located between the heat source and the displacement detection point. Both the Z-direction and X-direction converge quickly, but due to the fluctuation of the cooling water, the X-direction displacement of S3 has not been stable. The cooling effect and algorithm calculation results are sorted from high to low, as shown in Table 4. The Z-direction cooling effect is S1>S3>S5>S4>S2, and the X-direction cooling effect is S1>S3>S4>S5>S2. The experimental results and algorithm calculation results show that the cooling effect of the temperature-sensitive points T1 (S1) and T4 (S3) are the best, and the cooling effect of the T3 (S2) point is the worst, which verifies the accuracy of the algorithm and the feasibility of cooling the temperature-sensitive points.

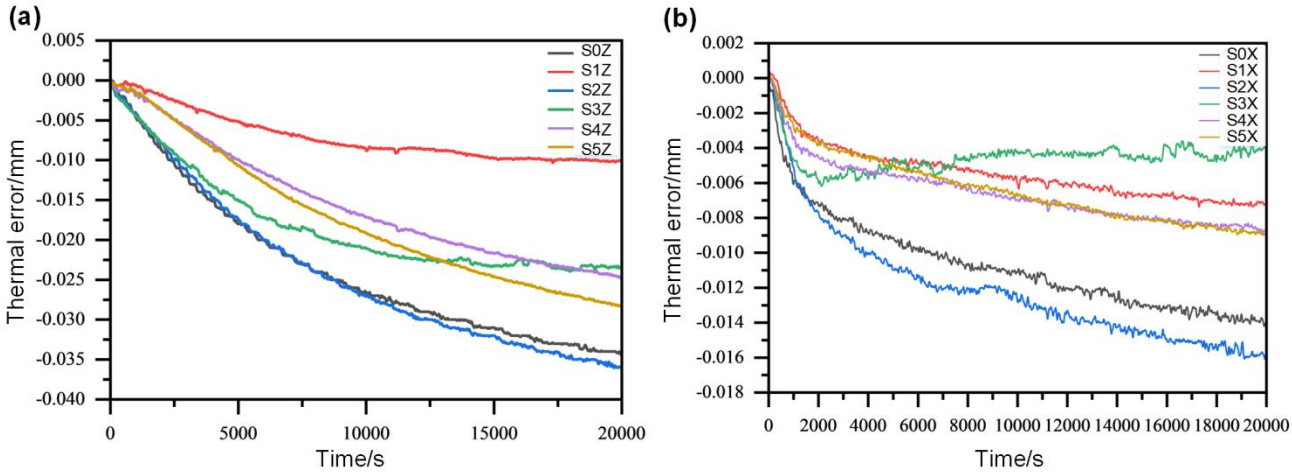

Fig. 12 Data analysis of the cooling experiment **(a)** Shell Z-direction thermal error **(b)** Shell X-direction thermal error

Table 4 Cooling effect and algorithm comparison

Cooling effect	Z-direction		X-direction	
	Cooling effect	Algorithm calculation result	Cooling effect	Algorithm calculation result
Excellent	S1	T1（S1）	S1	T1（S1）
	S3	T4（S3）	S3	T4（S3）
	S5	T11（S5）	S4	T8（S4）
	S4	T8（S4）	S5	T11（S5）
Poor	S2	T3（S2）	S2	T3（S2）

5. Conclusion

In this paper, considering that the suppression of different temperature-sensitive points during the cooling process has different cooling effects on the cooling of the milling head, the sensitivity analysis algorithm combined with the randomized mean value method is adapted to screen out the temperature-sensitive points, and the thermal error cooling suppression experiment is carried out. Finally come to the following conclusions:

(1) From the thermal-structure coupling simulation of the milling head, it can be obtained that the

maximum temperature of the milling head is located at the rotor of the motorized spindle, the maximum deformation is at the end of the motorized spindle, and the maximum temperature of the shell is located at the bottom of hole A, which has a greater impact on the X-direction thermal error of the end of the motorized spindle. The temperature field of the shell has little effect on the Y-direction displacement of the end of the motorized spindle.

(2) The randomized mean value method is introduced into the BP neural network sensitivity analysis algorithm, which can reduce the instability of the neural network sensitivity analysis to a certain extent, and make the parameter sensitivity analysis results of the neural network model have a better consistency.

(3) Compared with the uncooled state, the points with higher sensitivity coefficients can achieve a better suppression effect after cooling, and the temperature-sensitive point S1 can simultaneously reduce the thermal error in both X and Z-directions by about 58%. It is shown that the optimization of temperature measurement points can accurately find temperature-sensitive points.

(4) If the locations of the temperature-sensitive points are accurately identified in the design stage, the enterprise can directly modify and optimize the structural design and related parameters of the milling head or add a cooling system and a heat dissipation system at the temperature-sensitive points to achieve the purpose of reducing thermal deformation and improving machining accuracy.

Statements and Declarations

Funding This work is funded by the National Natural Science Foundation of China (No.52075134); the Opening Project of the Key Laboratory of Advanced Manufacturing and Intelligent Technology Ministry of Education, Harbin University of Science and Technology (No. KFKT202105); the Joint Guidance Project of Natural Science Foundation of Heilongjiang Province of China (No. LH2019E062); the Special Funding for Postdoctoral Fellows in Heilongjiang Province of China (No. LBH-Q20097).

Author contribution All authors contributed to the study conception and design. Material preparation, experimental verification, data collection and analysis were performed by Ye Dai, Zhaolong Li, Wanjian Wen and Shiqiang Zhan. The first draft of the manuscript was written by Yang Li and all authors commented on previous versions of the manuscript. All authors read and approved the final manuscript.

Availability of data and material Not applicable

Competing Interests The authors have no relevant financial or non-financial interests to disclose.

References

[1] Zhang L, Liu CS, LiY, Kong XZ, Mang ZL (2011) Application of a hydraulic brake mechanism in milling head with double rotary-swivel axses. Mach Tool Hydrau 39(24): 11-12

[2] Fu GQ, Gong HW, Fu JZ, Gao HL, Deng XL (2019) Geometric error contribution modeling and

sensitivity evaluating for each axis of five-axis machine tools based on POE theory and transforming differential changes between coordinate frames. Int J Mach Tool Manu 147:103455

[3] Fu JZ, Yao XY, He Y, Shen HY (2010) Development of Thermal Error Compensation Technology for NC Machine Tool. Aeron Manuf Technol (4):3

[4] Sun YH, Xiao W, Hu RK, Huang MF (2014) Thermal characteristics analysis of mill head of five-axis CNC mill machine based on finite element method. Appl Mech Mater 446-447: 509-512

[5] Zhao C, Xia Y, Chen X, Jiang Y, Fei Y (2020) Thermal error detection and compensation technology for spindle of horizontal CNC machine tool with large torque. Int J Adv Manuf Tech 107(1): 85-96

[6] Liu T, Gao W G, Zhang DW, Zhang YF, Chang WF, Liang CM, Tian YL (2017) Analytical modeling for thermal errors of motorized spindle unit. Int J Mach Tool Manu 112:53-70

[7] Lin JF, Yan M, Zheng P, Sun SX (2010) Finite element analysis of transmission components of C for direct-drive bi-rotary angle milling head. Journal of Mechanical Transmission 34(5): 59-61

[8] Zhou C, Qu Z, Hu B, Li S (2021) Thermal network model and experimental validation for a motorized spindle including thermal-mechanical coupling effect. Int J Adv Manuf Tech 1-15

[9] Ke Y, Hong J, Zhang J, Wei M, Wu W (2016) Thermal-deformation coupling in thermal network for transient analysis of spindle-bearing system. Int J Therm Sci 104:1-12

[10] Guo QJ, Fan S, Xu RF, Cheng X, Zhao GY, Yang JG (2017) Spindle thermal error optimization modeling of a five-axis machine tool. Chinese Journal of Mechanical Engineering 30(3): 746-753

[11] Abdulshahed AM, Longstaff AP, Fletcher S, Myers A (2015) Thermal error modelling of machine tools based on ANFIS with fuzzy C-means clustering using a thermal imaging camera. Appl Math Model 39(7): 1837-1852

[12] Wu CY, Xiang ST, Xiang WS (2021) Thermal error modeling of rotary axis based on convolutional neural network. J Manuf Sci Eng 143(5): 1-13

[13] Li S, Mei SK, Yuai W, Guo QJ (2020) Dynamic error model of five-axis machine tool based on AFSA-ACO-BPN algorithm. Mach Tool Hydrau 48(4): 141-145

[14] Tunkiel AT, Sui D, Wiktorski T (2020) Data-driven sensitivity analysis of complex machine learning models: A case study of directional drilling. J Pet Sci Eng 2020:107630

[15] Arnst M, Ponthot JP (2013) A probabilistic characterization, propagation, and sensitivity analysis of uncertainties in a metal forming application. J Korean Phys Soc 64(12):1814-1818

[16] Guo SJ, Zhang DS (2020) Geometric error analysis and compensation of rotary axis of five-axis machine tool. Advanced Engineering Sciences 52(2): 130-139

[17] Jiang DG, Quan XF, Yao YZ, Liu W (2019) Sensitivity analysis on input factors of chlorophyll a content neural network prediction model based on randomization method. Water Resour Hydr Eng 50(5):175-181

[18] Yang H, Fang H, Liu LX, Zhang DJ, Yin GF, Xu DW (2011) Method of key thermal stiffness

identification on a machine tool based on the thermal errors neural network prediction model. Journal of Mechanical Engineering 47(11):117-124

[19] Guo TN, Rong W, Liu ZF, Li FP, Yang WT, Dong X (2011) Thermal Characteristics Analysis on Large Torque and High Capacity Angular Milling Head. J Beijing Univ Technol 37(5):8

[20] Garson GD (1991) Interpreting neural-network connection weights. AI Expert 4(6): 47

[21] Olden JD, Joy MK, Death RG (2014) An accurate comparison of methods for quantifying variable importance in artificial neural networks using simulated data. Ecol Modell 178(3-4): 389-397